Mechanism of RAD51-Dependent DNA Interstrand Cross-Link Repair

David T. Long *et al.*

Science **333**, 84 (2011);
DOI: 10.1126/science.1204258

18. D. D. P. Johnson, *J. Wash. Acad. Sci.* **95**, 89 (2009).
19. R. D. Sagarin *et al.*, *Nature* **465**, 292 (2010).
20. J. Rudnick, G. Gaspari, *Elements of the Random Walk* (Cambridge Univ. Press, Cambridge, 2010)
21. D. Ben-Avraham, S. Havlin, *Diffusion and Reactions in Fractals and Disordered Systems* (Cambridge Univ. Press, Cambridge, 2000)
22. N. F. Johnson, P. Jefferies, P. M. Hui, *Financial Market Complexity* (Oxford Univ. Press, Oxford, 2003), p. 20.
23. J. Bohannon. *Science* **331**, 1256 (2011).

Acknowledgments: The authors gratefully acknowledge support for this research from the Joint IED Defeat Organization, IDN# N70465, and from The MITRE Corporation and the Santa Fe Institute for their co-hosting of the "Mathematics of Terrorism" workshop. The views and conclusions contained in this paper are those of the authors and should not be interpreted as representing the official policies, either expressed or implied, of any of the above named organizations, to include the U.S. government. We also thank P. Dodds, C. Danforth and A. Clauset for broad discussions surrounding this topic, L. Amaral for discussions concerning non-Poissonian behavior, and the anonymous reviewers for suggestions.

Supporting Online Material
www.sciencemag.org/cgi/content/full/333/6038/81/DC1
SOM Text
Figs. S1 to S3
SOM Data Analysis

2 March 2011; accepted 26 May 2011
10.1126/science.1205068

Mechanism of RAD51-Dependent DNA Interstrand Cross-Link Repair

David T. Long,[1] Markus Räschle,[2] Vladimir Joukov,[3] Johannes C. Walter[1]*

DNA interstrand cross-links (ICLs) are toxic DNA lesions whose repair in S phase of eukaryotic cells is incompletely understood. In *Xenopus* egg extracts, ICL repair is initiated when two replication forks converge on the lesion. Dual incisions then create a DNA double-strand break (DSB) in one sister chromatid, whereas lesion bypass restores the other sister. We report that the broken sister chromatid is repaired via RAD51-dependent strand invasion into the regenerated sister. Recombination acts downstream of FANCI-FANCD2, yet RAD51 binds ICL-stalled replication forks independently of FANCI-FANCD2 and before DSB formation. Our results elucidate the functional link between the Fanconi anemia pathway and the recombination machinery during ICL repair. In addition, they demonstrate the complete repair of a DSB via homologous recombination in vitro.

In vertebrate cells, DNA interstrand cross-link (ICL) repair is coupled to DNA replication and involves structure-specific endonucleases, translesion DNA polymerases, recombinases, and numerous proteins mutated in the human disease Fanconi anemia (FA) (*1*). FA is characterized by genomic instability and cellular sensitivity to DNA interstrand cross-linking agents. A central event in the FA pathway is the ubiquitylation of the FANCI-FANCD2 heterodimer, which activates it for ICL repair (*2*, *3*). Extensive evidence indicates that homologous recombination (HR) is essential for ICL repair (*4*–*9*). However, the precise role of HR in ICL repair remains conjectural, and the functional connection between the FA and HR pathways is unclear.

Using *Xenopus* egg extracts, we established a cell-free system for replication-dependent repair of a plasmid containing a single, site-specific cisplatin ICL (pICL) (Fig. 1A) (*2*, *10*). Upon addition of pICL to egg extracts, replication initiates at a random site, and two replication forks converge on the ICL (Fig. 1B, i). The leading strand of one fork is then extended to within one nucleotide of the ICL (Fig. 1B, ii). Next, dual incisions surrounding the ICL create a DNA double-strand break (DSB) in one sister chromatid, and translesion DNA synthesis restores the other sister by first inserting a nucleotide across from the adducted base (Fig. 1B, iii), followed by strand extension beyond the ICL (Fig. 1B, iv). Ultimately, 5 to 25% of replicated pICL is fully repaired, as measured by regeneration of a SapI site that was originally interrupted by the cross-link (*2*, *10*). In the absence of ubiquitylated FANCD2, DNA incisions, lesion bypass, and SapI site regeneration are greatly diminished (*2*). Given the established links between HR and ICL repair and the inefficient removal of the unhooked ICL in egg extracts (*10*), we postulated that SapI site regen-

[1]Department of Biological Chemistry and Molecular Pharmacology, Harvard Medical School, Boston, MA 02115, USA. [2]Department of Proteomics and Signal Transduction, Max Planck Institute of Biochemistry, 82152 Martinsried, Germany. [3]Department of Cancer Biology, Dana-Farber Cancer Institute, Boston, MA 02115, USA.

*To whom correspondence should be addressed. E-mail: johannes_walter@hms.harvard.edu

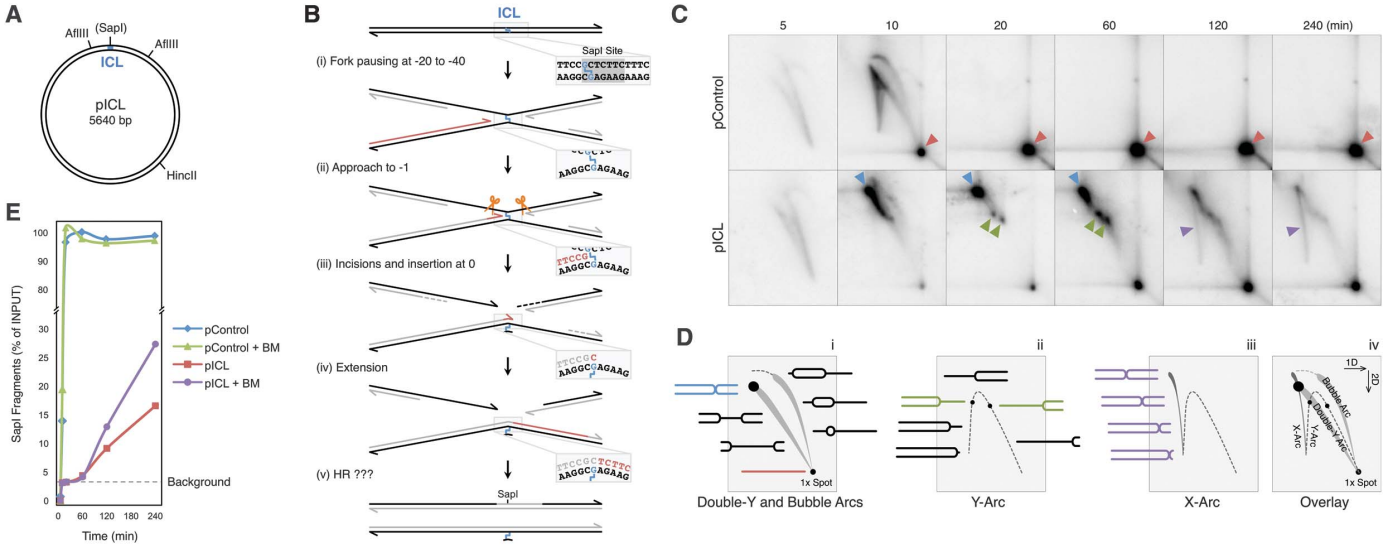

Fig. 1. The X-arc contains intermediates of ICL repair. (**A**) pICL schematic. (**B**) Model of ICL repair in *Xenopus* egg extracts (*2*, *10*). (**C**) pControl or pICL was replicated in egg extract, digested with HincII, and analyzed by 2DGE. Arrowheads, see main text. (**D**) Cartoon of 2DGE patterns and relevant DNA intermediates. (**E**) ICL repair of samples from (C) was analyzed under normal and branch migration (+BM) conditions. Background, SapI fragments from contaminating un–cross-linked plasmid. For primary data, see fig. S1, E and F. All graphed experiments were performed at least three times, and a representative example is shown.

eration involves repair of the broken sister chromatid by recombination with the intact sister (Fig. 1B, v).

To look for evidence of HR in ICL repair, pICL or an undamaged control plasmid (pControl) was replicated in egg extract, digested with HincII (Fig. 1A), and analyzed by two-dimensional gel electrophoresis (2DGE) (Fig. 1, C and D) (*11*). After 5 min, both plasmids generated the expected double-Y and bubble replication intermediates (Fig. 1C and Fig. 1D, i). As replication neared completion, pControl produced unit-sized linear DNA molecules (Fig. 1C, red arrowheads, and Fig. 1D, i), whereas pICL yielded a discrete X-shaped intermediate that results from the convergence of two forks on the ICL (Fig. 1C, blue arrowheads, and Fig. 1D, i). Two simple-Y intermediates also accumulated (3 to 7% of total signal), suggesting that a small number of converging forks undergo aberrant breakage or cleavage (Fig. 1C, green arrowheads, and Fig. 1D, ii). By 60 min, the X-shaped intermediates showed signs of processing, likely due to resection of the nascent lagging strands (*10*). Even later, the X- and Y-shaped intermediates were replaced by an "X-arc" (Fig. 1C, purple arrowheads, and Fig. 1D, iii). Formation of the X-arc coincided with SapI site regeneration (Fig. 1E, red trace), suggesting that the X-arc contains intermediates of ICL repair.

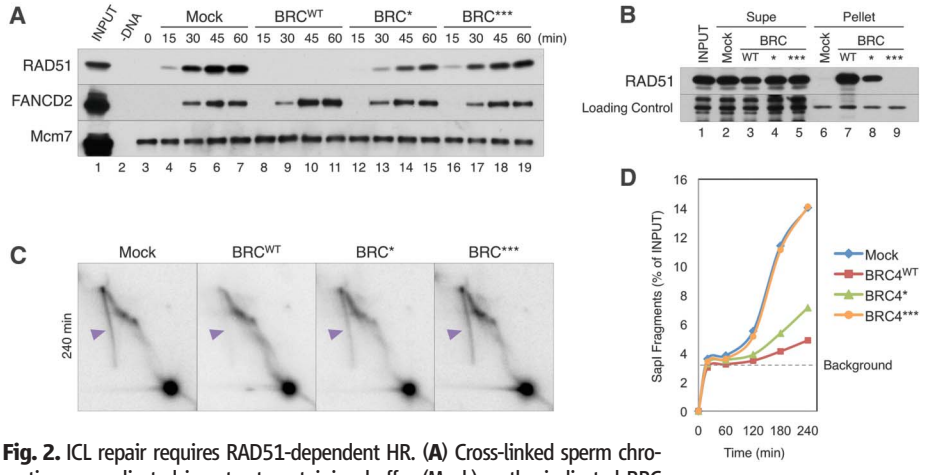

Fig. 2. ICL repair requires RAD51-dependent HR. (**A**) Cross-linked sperm chromatin was replicated in extract containing buffer (Mock) or the indicated BRC peptide, and chromatin-associated proteins were analyzed by Western blotting. (**B**) BRC peptides immobilized on glutathione sepharose beads were incubated with egg extract (*13*), pulled down, and the supernatant (Supe) and pellet blotted for RAD51. (**C**) pICL was replicated in extract containing buffer (Mock) or the indicated BRC peptide. Samples were digested with HincII and analyzed by 2DGE. Purple arrowheads, X-arc position. (**D**) Samples from (C) were analyzed for ICL repair as in Fig. 1E.

X-arcs are generally formed when two unit-sized linear molecules are joined by a mobile branch point, such as a Holliday junction or hemicatenane (Fig. 1D, iii) (*12*). Under conditions that promote resolution of mobile junctions through branch migration (*13*), the X-arc intermediates of pICL were resolved primarily into the predicted unit-sized linear molecules, whether magnesium was present or not (fig. S1, A to C). Magnesium inhibits migration of Holliday junctions, which implies that the X-arc intermediates contain hemicatenanes. Consistent with this, X-arc intermediates were resistant to cleavage by the Holliday junction resolvase, RuvC (fig. S1D). Exposing replicated pICL to branch migration conditions increased the yield of SapI repair fragments (Fig. 1E, purple trace), further indicating that X-arcs contained intermediates of ICL repair.

If repair of pICL involves HR, inhibiting the RAD51 recombinase should block repair. To test this prediction, we used a ~35–amino acid "BRC" peptide derived from BRCA2 that binds RAD51 and, when supplied at high concentrations, inhibits RAD51 nucleoprotein filament formation (*14*). As recently reported (*15*), addition of a BRC^{WT} (where WT is wild type) peptide (fig. S2A) to *Xenopus* egg extracts abolished RAD51 loading onto damaged chromatin (Fig. 2A). Two variants of the peptide that were mutated in one (BRC*) or three (BRC***) amino acids (fig. S2A) were increasingly compromised for RAD51 binding (Fig. 2B) and inhibition of RAD51 loading (Fig. 2A), demonstrating that BRC^{WT} specifically targets RAD51. Without affecting DNA replication (fig. S2B), the BRC peptides inhibited X-arc formation proportional to their effect on RAD51 binding and filament formation (compare Fig. 2, A and B, with Fig. 2C). Thus, X-arc intermediates are RAD51-dependent, indicating

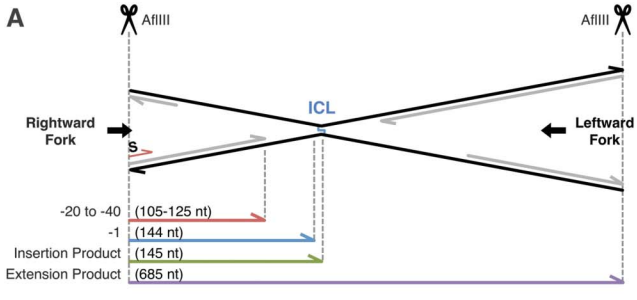

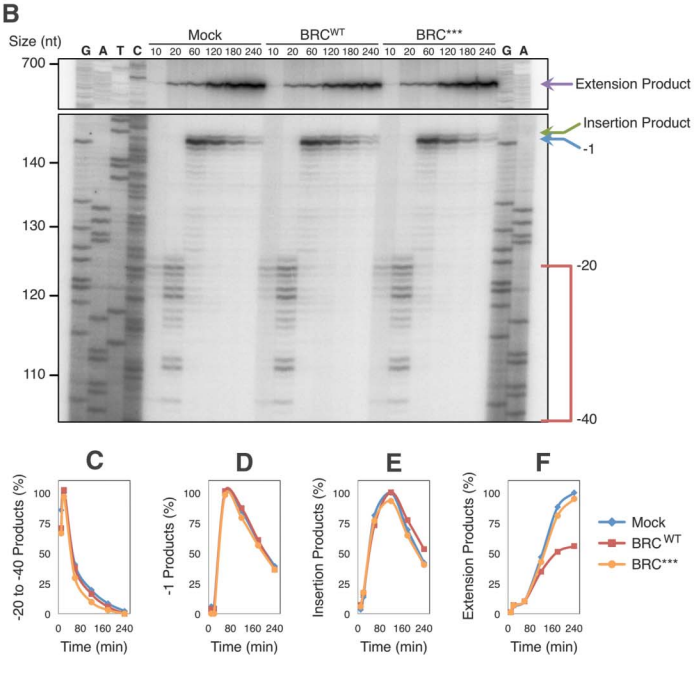

Fig. 3. RAD51-dependent HR functions at a late step in ICL repair. (**A**) Schematic depiction of leading strand intermediates from the rightward fork. (**B**) pICL was replicated in extract containing buffer (Mock) or the indicated BRC peptide. Samples were digested with AflIII and separated on a sequencing gel alongside a ladder generated with primer S [shown in (A)]. Nascent strands generated by the rightward fork are indicated at right. Products of the leftward fork gave the same result (not shown in this figure). The following products from (B) were quantified and graphed: (**C**) –20 to –40, (**D**) –1, (**E**) insertion, and (**F**) extension.

they represent products of HR. Although BRC^{WT} almost completely abolished SapI site regeneration, BRC* caused intermediate inhibition and BRC*** had no effect (Fig. 2D). These results demonstrate that replication-coupled ICL repair requires RAD51-dependent HR. Because dual incisions result in a two-ended DSB (Fig. 1B, iii), recombination likely first yields a double Holliday junction, which is then converted to a mobile hemicatenane.

We next used BRC peptides to investigate which step in ICL repair involves RAD51. Replicating pICL was digested with AflIII (Fig. 1A) and subjected to denaturing gel electrophoresis to examine leading strand products of the rightward and leftward replication forks as they converge on the ICL (Fig. 3A). In the presence of BRC^{WT}, the arrival of leading strands 20 to 40 nucleotides from the ICL (Fig. 3, B and C), the approach of leading strands to the –1 position (Fig. 3, B and D), and nucleotide insertion across from the adducted base (Fig. 3, B and E) were all unaffected. When BRC^{WT} samples were analyzed by native 1D- and 2DGE, there was no change in the rate at which dual-stalled fork structures disappeared (fig. S3, A to D), indicating that DNA incisions were unaffected. In contrast, BRC^{WT} specifically reduced full-length extension products twofold (Fig. 3, B and F), consistent with an absence of RAD51-mediated restoration of the broken sister chromatid (Fig. 1B, v). Timed addition of BRC peptides to ICL repair reactions indicated that RAD51 completes its repair function late, just before SapI site regeneration (fig. S4, A and B). Additionally, plasmid competition experiments showed that recombination occurred primarily between sister chromatids (fig. S5). Together, the data indicate that RAD51-dependent HR between the broken and intact sister chromatids is a crucial, late step in ICL repair.

We used chromatin immunoprecipitation (ChIP) to examine the binding of RAD51 and replication protein A (RPA) to three locations on pICL during repair (Fig. 4A). Initially, RPA and RAD51 accumulated near the ICL (Fig. 4B, site I). After a delay, they also bound ~700 base pairs from the ICL (Fig. 4B, site II), likely due to resection of lagging strands (*10*), but they never accumulated opposite the ICL (Fig. 4B, site III). No RAD51 binding was detected in the absence of replication, on undamaged plasmids, or in the presence of BRC^{WT} (fig. S6A). The timing of RPA binding coincided with the convergence of DNA replication forks at the lesion, followed shortly thereafter by RAD51 binding (Fig. 4C; green, blue, and red traces). When RAD51 binding peaked at 40 min, greater than 90% of the dual-stalled fork structures remained, indicating that little or no incisions had taken place (Fig. 4C, compare red and blue traces). To rule out the possibility that RAD51 binding at this time was limited to a small number of broken fork intermediates, we immunoprecipitated RAD51 from repair reactions and examined the associated DNA intermediates. Fifty-three percent of DNA associated with RAD51 consisted of intact, dual-stalled fork structures (Fig. 4D, red arrow). Thus, in the context of ICL repair, RAD51 is loaded onto stalled replication forks before DSB formation.

We next examined the connection between the FA and HR pathways. In FANCD2-depleted extracts, the X-arc disappeared, and it was rescued by readdition of recombinant FANCI-FANCD2 (Fig. 4E, purple arrowheads). As expected, the dual-stalled fork structure persisted in the absence of FANCD2 (Fig. 4E, blue arrowhead), consistent with a defect in incisions (*2*). The data indicate that HR acts downstream of FANCI-FANCD2 during ICL repair, explaining previous epistasis experiments (*7*). Consistent with some analyses of RAD51 foci [reviewed in (*8*)], RAD51 binding to ICLs was not reduced in the absence of FANCD2 (Fig. 4F and fig. S7, A to C). Conversely, inhibition of RAD51 function using BRC^{WT} peptide had no effect on FANCD2 recruitment or

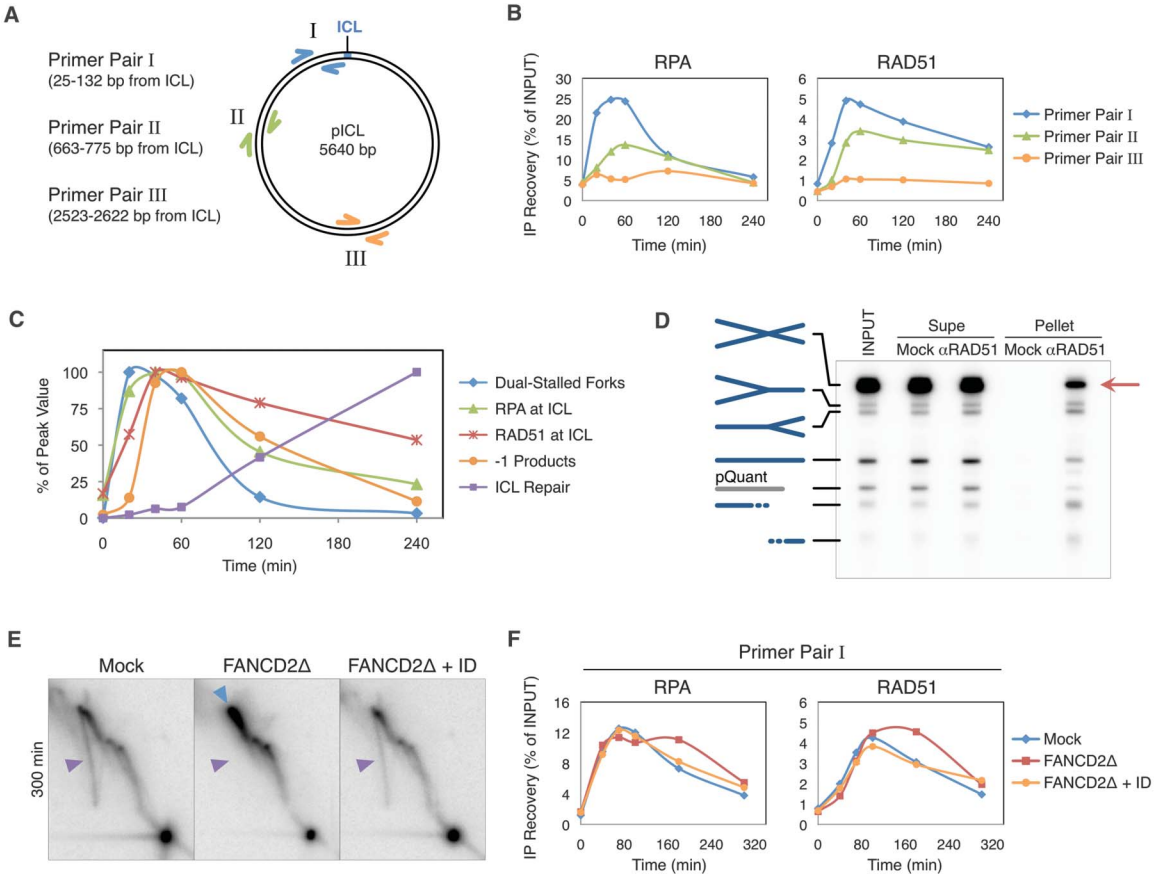

Fig. 4. Interplay between the HR and FA pathways. (**A**) Schematic of ChIP primer pairs. (**B**) pICL was replicated and analyzed by RPA and RAD51 ChIP. Controls containing BRC^{WT} peptide, pControl, or lacking DNA replication are shown in fig. S6A. (**C**) Samples from (B) were also analyzed for the timing of fork convergence, –1 product accumulation, and repair (raw data in fig. S6, B to D). The data were graphed as percentage of peak value and compared with RPA and RAD51 ChIP at site I [from (B)]. (**D**) pICL was replicated in extract for 40 min and immunoprecipitated with RAD51 antibodies (*13*). Recovered DNA was digested with HincII and analyzed by agarose gel electrophoresis. Repair intermediates are depicted at left for pICL (blue) and an internal control plasmid, pQuant (gray). Red arrow, see main text. (**E**) pICL was replicated in mock-depleted egg extract (Mock), FANCD2-depleted extract (FANCD2Δ), or FANCD2Δ extract supplemented with 375 nM FANCI-FANCD2 (FANCD2Δ+ID). Samples were digested with HincII and analyzed by 2DGE. Arrowheads, see text. See fig. S7E for complete 2D gel time courses. (**F**) Samples from (E) were analyzed by ChIP using primer pair I. Primer pairs II and III are shown in fig. S7A. IP, immunoprecipitation.

ubiquitylation (Fig. 2A and fig. S7D). Together, our data show that FANCI-FANCD2 acts upstream of HR in the context of replication-coupled ICL repair, but that it is not required for RAD51 recruitment to chromatin. Instead, the requirement for FANCI-FANCD2 in promoting HR can be explained by its role in promoting the incisions that underlie DSB formation (*2*). The FA pathway may also enhance HR via more direct mechanisms, because FA proteins also stimulate HR in the context of preformed DSBs (*6*, *7*, *9*, *16*, *17*).

Here, we report that in the context of replication-coupled ICL repair, the DSB generated in one sister chromatid through the action of FANCI-FANCD2 is fixed via strand invasion into the intact sister (fig. S8). We find that RAD51 binds efficiently to ICLs before a DSB has been generated (fig. S8, ii). Although lesion bypass likely displaces RAD51 from one sister chromatid, incisions and resection of the other sister creates a new docking site for RAD51, such that both ends of the DSB are coated with the recombinase (fig. S8, iv). The interaction of RAD51 with ICL-stalled forks before DSB formation may function to prevent fork breakage/degradation (*5*, *15*, *18*) in favor of regulated incisions and/or to initiate strand invasion as soon as possible once the DSB has been formed.

A major obstacle impeding our understanding of DSB repair has been the absence of cell-free systems. Combined with ChIP and the ability to inactivate or remove essential proteins, the system described here represents a powerful tool to elucidate the complex mechanism underlying DSB repair.

References and Notes

1. G.-L. Moldovan, A. D. D'Andrea, *Annu. Rev. Genet.* **43**, 223 (2009).
2. P. Knipscheer *et al.*, *Science* **326**, 1698 (2009); 10.1126/science.1182372.
3. W. Wang, *Nat. Rev. Genet.* **8**, 735 (2007).
4. A. J. Deans, S. C. West, *Mol. Cell* **36**, 943 (2009).
5. K. Nakanishi *et al.*, *Nat. Struct. Mol. Biol.* **18**, 500 (2011).
6. K. Nakanishi *et al.*, *Proc. Natl. Acad. Sci. U.S.A.* **102**, 1110 (2005).
7. W. Niedzwiedz *et al.*, *Mol. Cell* **15**, 607 (2004).
8. L. H. Thompson, J. M. Hinz, *Mutat. Res. Fundam. Mol. Mech. Mutagenesis* **668**, 54 (2009).
9. N. Zhang, X. Liu, L. Li, R. Legerski, *DNA Repair* **6**, 1670 (2007).
10. M. Räschle *et al.*, *Cell* **134**, 969 (2008).
11. M. Bzymek, N. H. Thayer, S. D. Oh, N. Kleckner, N. Hunter, *Nature* **464**, 937 (2010).
12. N. P. Robinson, K. A. Blood, S. A. McCallum, P. A. Edwards, S. D. Bell, *EMBO J.* **26**, 816 (2007).
13. Supplementary methods are available as supporting material on *Science* Online.
14. A. Carreira *et al.*, *Cell* **136**, 1032 (2009).
15. Y. Hashimoto, A. R. Chaudhuri, M. Lopes, V. Costanzo, *Nat. Struct. Mol. Biol.* **17**, 1305 (2010).
16. Y. G. Yang *et al.*, *Carcinogenesis* **26**, 1731 (2005).
17. K. Yamamoto *et al.*, *Mol. Cell. Biol.* **23**, 5421 (2003).
18. S. Lambert, B. Froget, A. M. Carr, *DNA Repair* **6**, 1042 (2007).

Acknowledgments: We thank V. Costanzo for the BRC^{WT} expression construct; T. V. Ho and O. Schärer for instruction on pICL preparation; P. Knipscheer for reagents and helpful discussions; and A. D'Andrea, K. J. Patel, R. Scully, and P. Knipscheer for critical reading of the manuscript. This work was supported by NIH grants GM GM80676 and HL098316 and a John and Virginia Kaneb award to J.C.W., Department of Defense Breast Cancer Research Program Award W81XWH-04-1-0524 to V.J., and American Cancer Society postdoctoral fellowship PF-10-146-01-DMC to D.T.L. M.R. made initial observation of X-arcs; V.J. generated *x.l.*RAD51 antibodies; D.T.L. and J.C.W. designed and analyzed experiments; D.T.L. performed experiments; and D.T.L. and J.C.W. prepared the manuscript.

Supporting Online Material

www.sciencemag.org/cgi/content/full/333/6038/84/DC1
Methods
Figs. S1 to S9
References

14 February 2011; accepted 12 May 2011
10.1126/science.1204258

A Key Enzyme in the Biogenesis of Lysosomes Is a Protease That Regulates Cholesterol Metabolism

Katrin Marschner,[1] Katrin Kollmann,[1] Michaela Schweizer,[2] Thomas Braulke,[1]* Sandra Pohl[1]

Mucolipidosis II is a severe lysosomal storage disorder caused by defects in the α and β subunits of the hexameric *N*-acetylglucosamine-1-phosphotransferase complex essential for the formation of the mannose 6-phosphate targeting signal on lysosomal enzymes. Cleavage of the membrane-bound α/β-subunit precursor by an unknown protease is required for catalytic activity. Here we found that the α/β-subunit precursor is cleaved by the site-1 protease (S1P) that activates sterol regulatory element–binding proteins in response to cholesterol deprivation. S1P-deficient cells failed to activate the α/β-subunit precursor and exhibited a mucolipidosis II–like phenotype. Thus, S1P functions in the biogenesis of lysosomes, and lipid-independent phenotypes of S1P deficiency may be caused by lysosomal dysfunction.

More than 50 soluble enzymes are targeted to lysosomes in a mannose 6-phosphate (M6P)–dependent manner. The formation of M6P residues on newly synthesized lysosomal enzymes is catalyzed by two multimeric enzyme complexes, *N*-acetylglucosamine (GlcNAc)-1-phosphotransferase and GlcNAc-1-phosphodiester-α-*N*-acetylglucosaminidase, allowing binding of the enzymes to M6P-specific receptors (*1*). The receptor-enzyme complexes are then transported to the endosomal compartment, followed by low pH–induced dissociation and delivery of lysosomal proteins to lysosomes and recycling of receptors to the Golgi apparatus. The GlcNAc-1-phosphotransferase comprises a hexameric complex of three subunits ($\alpha_2\beta_2\gamma_2$) with a molecular mass of 540 kD (*2*). The α and β subunits are encoded by a single gene, *GNPTAB*, and synthesized as a 190-kD precursor protein in a hairpin orientation that contains cytosolic N and C termini and a complex lumenal modular structure (*3*, *4*). Mutations in *GNPTAB* cause a severe lysosomal storage disorder, mucolipidosis II (MLII; I-cell disease) (*3*, *5*). The loss of GlcNAc-1-phosphotransferase activity leads to the synthesis of lysosomal enzymes lacking M6P residues, resulting in missorting and intracellular deficiencies of multiple lysosomal hydrolases, and lysosomal storage of nondegraded material, which are used as diagnostic markers in MLII patients (*6*). Clinically, these patients are characterized by skeletal abnormalities, chondrodysplasia, cardiomegaly, and motor and mental retardation, leading to early death (*6*). Cleavage of the α/β-subunit precursor between Lys^{928} and Asp^{929} by an unknown protease is a prerequisite for the enzymatic activity of the GlcNAc-1-phosphotransferase complex (*7*). Treatment with brefeldin A, a drug that disrupts Golgi trafficking, prevents the cleavage of the α/β-subunit precursor, suggesting that this reaction takes place in the Golgi apparatus (*8*).

To identify the protease responsible for the cleavage, we generated an α/β-subunit precursor miniconstruct that allows its efficient expression, spans the membrane twice, and lacks amino acids 431 to 819 (Fig. 1A). Antibodies to the human β subunit (*9*) allowed the detection of both the α/β-subunit precursor constructs and the cleaved 45-kD β subunit in baby hamster kidney (BHK) cells (Fig. 1B). Analysis of additional miniconstructs with stepwise deletions showed that 20 amino acids proximal to the cleavage site were required for proper proteolysis (Fig. 1B). Construct 3 was the best substrate and was used for all further experiments. To define structural requirements for efficient cleavage of the α/β-subunit precursor in more detail, we substituted residues Thr^{923} to Ser^{934} (according to the numbering of the full-length precursor) individually with alanines. Arg^{925}, Leu^{927}, and Lys^{928} were the most critical for cleavage of the phosphotransferase

[1]Department of Biochemistry, Children's Hospital, University Medical Center Hamburg-Eppendorf, Hamburg, Germany. [2]Department of Electron Microscopy, Center for Molecular Neurobiology, Hamburg, Germany.

*To whom correspondence should be addressed. E-mail: braulke@uke.uni-hamburg.de